Structure, optical properties and thermal stability of pulsed sputter deposited high temperature $HfO_x/Mo/HfO_2$ solar selective absorbers

N. Selvakumar, Harish C. Barshilia[a)], and K. S. Rajam
Surface Engineering Division, National Aerospace Laboratories (CSIR), Bangalore–560 017, India

A. Biswas
Applied Spectroscopy Division, Bhabha Atomic Research Center, Mumbai–400 085, India

Abstract

Solar selective coatings of $HfO_x/Mo/HfO_2$ were deposited on copper (Cu) and stainless steel (SS) substrates using a magnetron sputtering system. The HfO_x and HfO_2 layers were deposited from the sputtering of Hf target in $Ar+O_2$ plasma using an asymmetric bipolar-pulsed direct current generator. Whereas, the Mo layer was deposited from the sputtering of Mo target in the Ar plasma. The optimized $HfO_x/Mo/HfO_2$ multilayer absorber on Cu substrate exhibited high solar absorptance (α = 0.905-0.923) and low thermal emittance (ε = 0.07-0.09). Similarly, on SS substrates the optimized coatings exhibited α and ε in the ranges of 0.902-0.917 and 0.15-0.17, respectively. The X-ray diffraction data showed that the $HfO_x/Mo/HfO_2$ coating consists of tetragonal and monoclinic phases of HfO_2, which was confirmed by micro-Raman spectroscopy data. The bonding structure of the HfO_x and the HfO_2 layers were confirmed using X-ray photoelectron spectroscopy data. The optical constants (*n* and *k*), measured using spectroscopic ellipsometry, showed that the top HfO_2 layer acts as an antireflection coating and the bottom two layers (HfO_x and Mo) are the main absorber layers. The analysis of the spectroscopic

[a)]Author to whom correspondence should be addressed
Electronic mail: harish@nal.res.in
Fax # +091-80-2521 0113

ellipsometric data indicated that the band gap of the HfO_x and the HfO_2 layers were 3.90 and 5.82 eV, respectively, indicating non-stoichiometric nature of HfO_x. In order to study the thermal stability of the $HfO_x/Mo/HfO_2$ coatings, they were subjected to heat treatment in air and vacuum at different temperatures (T_A). The $HfO_x/Mo/HfO_2$ coatings deposited on Cu substrates were thermally stable up to 400°C for 2 h in air. Addition of a thin Mo interlayer (40 nm) in the $HfO_x/Mo/HfO_2$ coating (i.e., $Mo/HfO_x/Mo/HfO_2$) deposited on Cu substrates exhibited high solar selectivity (α/ε) of 0.872/0.09 even after heat-treatment in air up to 500°C for 2 h. At T_A = 525°C, the solar selectivity decreased drastically (α/ε = 0.761/0.35) due to the formation of MoO_2, MoO_3 and $HfMo_2O_8$ phases. The $Mo/HfO_x/Mo/HfO_2$ coatings deposited on SS substrates showed no significant changes in α and ε values after annealing at 500°C in air and at 800°C in vacuum. These results were confirmed by micro-Raman spectroscopy measurements, which showed the compositional stability of these coatings up to 500°C in air and 800°C in vacuum.

I. Introduction

Transition metal oxide coatings such as Cr_2O_3, MoO_3, WO_x, etc. have been used for solar selective applications due to their excellent optical properties and good thermal stability.[1] The optical properties of transition metal based coatings can be tailored by controlling the stoichiometry, which affects the density of free electrons in the *d* band.[1] Among transition metal oxides, especially hafnium oxide (HfO_2) coatings are technologically important because of their good mechanical, chemical and thermal stability as well as relatively high dielectric constant and high refractive index (*n*).[2] The wide band gap (5.5 eV) of HfO_2 gives it transparency over a wide spectral range, extending from the ultraviolet to the mid-infrared (IR).[3] Due to its large band gap and high refractive index, HfO_2 is an interesting candidate for optical applications. HfO_2 is used as an optical coating for astronomically charged coupled devices[4], antireflective multilayer coating for night vision devices[5], high reflectivity mirrors and for IR optical devices.[6,7]

The optical properties of single layer hafnium oxide thin films have been studied extensively.[8-11] Khoshman and Kordesch reported that amorphous HfO_2 films exhibited high transmittivity (80-97%) and low reflectivity (< 15%) in the visible and the near IR regions, respectively.[8] Park et al. have reported that the optical properties of HfO_2 films are directly correlated with the crystal structure of HfO_2.[9] Al-Kuhaili developed hafnium oxide based heat mirror (HfO_2/Ag/ HfO_2), which exhibited an average transmittance of 72.4% in the wavelength range of 700-2000 nm.[3] He also reported that the HfO_2 based heat mirror can be used for energy efficient window applications. To the best of our knowledge, HfO_2 based multilayer absorber coatings for high temperature solar thermal applications have not been developed and studied so far. Detailed studies regarding the absorptance and the thermal stability of the HfO_2

based coatings are lacking. We have investigated the possibility of designing a dielectric/metal/dielectric (D/M/D) multilayer absorber coating of HfO_2 and molybdenum.

The HfO_2 coatings have been mainly prepared by electron beam evaporation, atomic layer deposition, pulsed laser deposition, chemical vapor deposition and sputtering methods.[2,3,8,9,12,13] In most of the sputter deposited HfO_2 coatings, reactive direct current (DC) and radio frequency (RF) sputtering methods have been used. DC sputtering has serious limitations for the sputtering of oxides and RF sputtering suffers from low growth rates and its complexity. Recently, pulsed sputtering has been developed for the deposition of highly adherent, uniform and dense coatings of dielectric nitrides and oxides with high growth rates.[14] Asymmetric bipolar-pulsed DC generators have been successfully used for the deposition of insulating films from the reactive sputtering of metal targets.

In the present work, we have designed an $HfO_x/Mo/HfO_2$ multilayer absorber coating with high absorptance and low emittance for high temperature solar applications. Asymmetric bipolar-pulsed DC generator was used to develop the $HfO_x/Mo/HfO_2$ multilayer absorber coatings on copper (Cu) and stainless steel (SS) substrates. By switching on and off the oxygen flow, alternate layers of hafnium oxide and molybdenum were deposited. The flow rate of oxygen was controlled manually by switching on and off the mass flow controller. In order to achieve the exact composition, each layer was deposited after stabilizing the plasma for five minutes during which a shutter was used in between the substrate and the target. The structural, chemical and optical properties of these coatings have been studied using X-ray diffraction (XRD), X-ray photoelectron spectroscopy (XPS), atomic force microscopy (AFM), micro-Raman spectroscopy, field emission scanning electron microscopy (FESEM), solar spectrum

reflectometer and emissometer and phase-modulated spectroscopic ellipsometry. We discuss in detail the thermal stability of these coatings in air and in vacuum.

II. EXPERIMENTAL DETAILS

$HfO_x/Mo/HfO_2$ coatings were prepared on Cu substrates (dimension: 35 mm × 35 mm × 2 mm) using a reactive DC unbalanced magnetron sputtering system.[14] Before putting the substrates into the vacuum chamber, they were metallographically polished and chemically cleaned. The vacuum chamber was pumped down to a base pressure of 5.0×10^{-4} Pa. High purity Hf (99.95%) and Mo (99.95%) targets (diameter = 0.075 m) were used for the deposition of the coatings. An asymmetric bipolar-pulsed generator (frequency = 100 kHz, pulse width = 2976 ns, positive pulse bias = +37 V) was used to sputter the Hf target.[14] The HfO_2 layer was prepared from the reactive sputtering of Hf target in Ar + O_2 plasma at a pressure of 1.0×10^{-1} Pa. For the deposition of the bottom HfO_x layer, the power density was 9 W/cm^2 and the oxygen flow rate was 6 sccm. The Mo metal layer was deposited from the non-reactive sputtering of the metal target in Ar plasma at a pressure of 1.0×10^{-1} Pa. Sputtering was carried out at a power density of 3.4 W/cm^2 for the Mo metal layer. For the top HfO_2 layer, the power density was 9 W/cm^2 and the oxygen flow rate was 8 sccm. All the coatings were deposited at a substrate temperature of approximately 40 – 50°C.

The absorptance (α) and emittance (ε) of the $HfO_x/Mo/HfO_2$ coatings were measured using solar spectrum reflectometer (Model SSR) and emissometer (Model AE) of M/s. Devices and Services. For the solar spectrum reflectometer, the source of the illumination was a tungsten-halogen lamp. The radiation reflected by the sample was measured at an angle of 20º from the normal, with four filtered detectors (UV, blue, red and infrared). By summing the four outputs in the appropriated proportions, a solar spectrum measurement was achieved. Air mass

2 was used to calibrate the solar reflectometer. The emissometer was heated to 82°C, so that the sample to be measured need not be heated. Both the instruments were calibrated using standard samples. This emissometer is a special purpose instrument to measure the emittance of absorber coatings used for flat plate solar thermal collector, wherein the maximum working temperature of the collector is of the order of 80-85 °C. At 82 °C, the spectral range of the thermal radiation emitted from the surface is in the range of 3-30 μm.[1] The detector in the emissometer consists of a differential thermopile with low and high emittance areas, which ensures near constant response to the emitted radiation in this wavelength range. The accuracies of the measured α values are ± 2% with a drift of ± 1% + 0.003/h and the emissometer has a repeatability of ± 0.01 units. The absorptance and the emittance values were measured at four different positions and the values reported herein are the average of four measurements. The ellipsometric data were measured in a spectroscopic phase modulated ellipsometer (Model UVISEL^{TM} 460, ISA JOBIN-YVON SPEX) in the wavelength range of 350-1200 nm.

XRD patterns of the coating were recorded in a Rigaku D/max 2200 Ultima X-ray powder diffractometer. The X-ray source was a Cu K_α radiation (λ = 0.15418 nm), which was operated at 40 kV and 30 mA. The bonding structure of the coatings was characterized by XPS using an ESCA 3000 (V.G. Microtech) system with a monochromatic Al K_α X-ray beam (energy = 1486.5 eV and power = 150 watts). The microstructure of the coatings was studied using field-emission scanning electron microscopy (Supra 40VP, Carl Zeiss). Approximately 10 nm thick gold coating was deposited on HfO_x/Mo/HfO_2 coatings for FESEM measurements. The surface roughness of the coatings was measured using atomic force microscopy (Surface Imaging Systems).

In order to test the thermal stability, the HfO_x/Mo/HfO_2 coatings deposited on copper and stainless steel substrates were heated in air in a resistive tubular furnace at temperatures in the range of 200-525ºC for 2 h. The hot zone of the furnace was 0.05 m in diameter and 0.05 m in length. The accuracy of the set temperature was ± 5ºC. Annealing involved increasing the temperature of the samples from room temperature to the desired temperature at a slow heating rate of 5°C/min and maintaining the desired temperature for 2 h. Subsequently, the samples were cooled down at a rate of 5°C/min. Changes in the chemical composition of the solar selective coatings as a result of heating were measured using micro-Raman spectroscopy. A DILOR-JOBIN-YVON-SPEX integrated Raman spectrometer (Model Labram) was used for the present experiments.[15] The spectrometer consisted of a microscope coupled confocally to a 300 mm focal length spectrograph equipped with two switchable gratings (300 and 1800 grooves/mm). A HeNe 20 mW laser beam was used as the excitation source. The laser was totally reflected by a notch filter towards the sample under a microscope and the Raman scattering was totally transmitted through the notch filter towards the confocal hole and entrance slit of the spectrometer. The spectrum was recorded in a Peltier cooled charge coupled devices detector. The data were collected with a 20 seconds data point acquisition time in the spectral range of 50-1100 cm^{-1}. The thermal stability of the coatings in vacuum (5.0×10^{-4} Pa) was also studied using micro-Raman spectroscopy. Molybdenum strips were used as heating elements to heat a stainless steel 316 thick plate, on which the test samples were placed. A diffusion pump was used to create the vacuum. The accuracy of the set temperature was ± 10ºC. A heating rate of 5°C/min and a cooling rate of 5°C/min were used.

III. RESULTS AND DISCUSSION

A. Design of HfO_x/Mo/HfO_2 multilayer absorbers

A multilayer absorber is a combination of single layers with different optical constants and film thicknesses. When an incident light falls on a multilayer absorber, the light interferes with one or more of the waves that are reflected from the various interfaces in the multilayer coatings.[16] Generally, light reflected from the interfaces will experience a 180° phase change when it is reflected from a medium of high refractive index and no phase change will occur, when it is reflected from a medium of low refractive index. The phases and the amplitudes of these waves determine whether the resultant sum of these waves lead to constructive/destructive interference and an increase/decrease in the reflectance of the incident light.[16]

A schematic diagram of the HfO_x/Mo/HfO_2 multilayer absorber coating deposited on Cu substrate is shown in Fig. 1. The coating consists of a semitransparent Mo metal layer (layer 2 – approximately 31 nm thick) sandwiched between HfO_2 and HfO_x layers. Molybdenum was used as a metal layer due to its high infrared reflectance and good solar absorptance.[17] Its low reflectance in the visible region, when compared to that of noble metals resulted in an increased solar absorptance. Furthermore, the high free electron density of molybdenum leads to high IR reflectivity which results in the desired low emittance in the infrared region.[17] The bottom absorber layer, HfO_x (layer 1- approximately 26 nm thick) is designed to have a lower oxygen content than the top HfO_2 layer (layer 3 - approximately 67 nm thick) in order to achieve different refractive indices for both the layers. The oxygen flow rate was varied in order to achieve the different composition (i.e., 6 sccm for HfO_x and 8 sccm for HfO_2 layer). The top HfO_2 layer has higher oxygen content and acts as an antireflection coating. This is because stoichiometric HfO_2 has a wide band gap (i.e., 5.82 eV) which gives it transparency over a wide spectral range (from ultraviolet to mid-infrared region). Whereas, the bottom HfO_x layer exhibits significant absorption in the visible region which was confirmed by the ellipsometry

data (explained below). The design of HfO_x/Mo/HfO_2 multilayer absorber is based on the idea that destructive interference (i.e., interference induced absorption) between adjacent layers leads to an increase in the solar absorptance. This was confirmed by the optical constants data and will be discussed later. The optimized HfO_x/Mo/HfO_2 coating deposited on Cu substrate exhibited a high absorptance of the order of 0.905-0.923 and a low emittance of 0.07-0.09 at 82 ºC.

B. Structural properties

Hafnium oxide exhibits several polymorphs such as monoclinic (*m*-) phase at room temperature and atmospheric pressure and orthorhombic and tetragonal (*t*-) phases at high pressures and/or high temperatures.[18] Fig. 2(a) shows the XRD pattern of the HfO_2 coating (approximately 1.0 μm thick) deposited at an oxygen flow rate of 8 sccm. The coating exhibited both tetragonal and monoclinic phases of HfO_2. The XRD pattern shows a high intensity peak centered at 2θ = 27.9º which corresponds to the $(\bar{1}11)$ plane of monoclinic phase of HfO_2. The weak and broad peaks centered at 35.54 and 44.6° correspond to the (200) and (211) planes of *m*-HfO_2, respectively.[19] Similarly, the peaks at 2θ = 31.6, 33.96 º, 38.36 º and 50.14º originate from the (111), (002), (102) and (220) planes of *t*-HfO_2, respectively.[20]

Fig. 2(b) shows the XRD pattern of a typical HfO_x/Mo/HfO_2 (approximately 125 nm thick) coating deposited on Si substrate. The XRD pattern shows low intensity peaks centered at 2θ = 38.32º and 44. 60º, which correspond to (102) plane of *t*-HfO_2 and (211) plane of *m*-HfO_2, respectively. The peak marked with "S" originates from the substrate. No peaks pertaining to crystalline Mo were observed in the XRD data. These results clearly indicate that the hafnium oxide present in the multilayer absorber coating exhibited a mixture of monoclinic and tetragonal phases.

C. Micro-Raman spectroscopy studies

Raman spectroscopy technique was used to characterize the HfO_x/Mo/HfO_2 coatings as the molecular vibration signatures from a Raman spectrum are very sensitive to chemical structure and bonding, rather than just atomic composition. Group theory predicts 36 phonon modes for *m*-HfO_2, in which 18 modes ($9A_g+9B_g$) are Raman active and 15 modes ($8A_u+7B_u$) are IR active, the remaining three modes being the zero-frequency translational modes. There are three IR active modes ($A_{2u}+2E_u$) and three Raman active modes ($A_{1g}+B_{1g}+E_g$) for *t*-HfO_2.[21] Fig. 3(a) shows the Raman spectrum of single layer HfO_2 coating deposited on Si substrates at an oxygen flow rate of 8 sccm. The spectrum of single layer HfO_2 coating shows three broad and diffused Raman bands centered at 316, 396 and 639 cm^{-1}. The band centered at 316 cm^{-1} is of A_g symmetry and the other bands centered at 396 and 639 cm^{-1} are attributed to B_g symmetry of *m*-HfO_2.[21] The peak centered at 521 cm^{-1} corresponds to silicon substrate. Fig. 3 (b) shows the Raman spectrum of a typical HfO_x/Mo/HfO_2 coating and the spectrum shows two strong bands centered at 170 and 210 cm^{-1} and two weak bands centered at 382 and 629 cm^{-1}. The exact position of various Raman bands was determine using deconvolution of the Raman data as shown in inset of Fig. 3. The bands centered at 170 and 382 cm^{-1} originate from B_g symmetry of *m*-HfO_2 and the other bands centered at 201 and 629 cm^{-1} may be attributed to E_g and A_{1g} symmetry, respectively of *t*-HfO_2.[21,22] It is worth noting that in the observed spectra, the number of Raman active vibrational modes identified is less than the number of the corresponding modes predicted from the group theory analysis for monoclinic HfO_2. This is due to the fact that the Raman active vibrations for HfO_2 have very close frequencies those cannot be separated in non-polarized Raman spectra of polycrystalline samples.[23]

D. X-ray photoelectron spectroscopy

Fig. 4(a-c) shows the core level XPS spectra of the single layer HfO_x (6 sccm-top layer) coating. The Hf 4f spectrum (Fig. 4(a)) of the HfO_x coating showed two peaks centered at 16.8 and 18.5 eV, which originate from Hf $4f_{7/2}$ and Hf $4f_{5/2}$, respectively of HfO_x.[24] Similarly, the Hf 4d (Fig. 4(b)) spectrum also showed two peaks centered at 213.4 and 224.2 eV corresponding to Hf $4d_{5/2}$ and Hf $4d_{3/2}$, respectively of HfO_x. The higher binding energies of the HfO_x coating suggest that the hafnium oxide coating was O-deficient, which confirms the formation of non-stoichiometric HfO_x.[24] The O 1s spectrum (Fig. 4(c)) showed a characteristic peak at a binding energy of 530.4 eV, which corresponds to O-Hf bonding.[24]

Fig. 4(d-f) shows core level XPS spectra of the HfO_2 (8 sccm-bottom layer) coating. The Hf 4f spectrum (Fig. 4(d)) of the HfO_2 coating showed two peaks centered at 16.4 and 18.0 eV, which originate from Hf $4f_{7/2}$ and Hf $4f_{5/2}$, respectively of HfO_2.[24] The shift in the binding energy towards the lower side and the doublet separation of 1.6 eV clearly indicates the formation of stoichiometric HfO_2. Similarly, the Hf 4d (Fig. 4(e)) spectrum also showed two peaks centered at 212.9 and 223.6 eV which correspond to Hf $4d_{5/2}$ and Hf $4d_{3/2}$, respectively of HfO_2. The O 1s spectrum (Fig. 4(f)) showed a characteristic peak at a binding energy of 530.1 eV, which corresponds to oxygen in HfO_2.[24] It has been reported that fully oxidized metal oxide has lower binding energy (HfO_2-530.1 eV) than that of oxygen deficient oxide (HfO_x-530.4 eV).[25]

E. Optical properties

Fig. 5 shows the experimental ψ (amplitude ratio of parallel and perpendicular components of the reflected waves) and Δ (relative phase change) spectra obtained by spectroscopic phase modulated ellipsometry over a wavelength range of 350-1200 nm for the HfO_x/Mo/HfO_2 coating on Cu substrate. The above experimental spectra were fitted with a three

layer model. The HfO_x and the HfO_2 layers were modeled using Adachi's model[26-28] and the middle metallic Mo layer was modeled using Cauchy's formula[29] for generating refractive indices (n) and extinction coefficients (k) spectra.[26-29] The fitting details are described elsewhere in our previous work.[28-31]

The theoretically generated spectra were fitted with experimentally measured ellipsometric spectra by varying thickness and parameters of dispersion relation of every layer for extracting the thickness, refractive indices and extinction coefficients of different layers. The fitting parameters for HfO_x and HfO_2 layers are shown in Table I, where A_{0x} is exciton strength parameter, G_0 is exciton binding energy, ε_∞ is the higher energy component of the dielectric constant, A_0 is the modulation amplitude, E_0 is the energy gap between bottom of conduction band and top of the valence band and Γ_0 is the broadening energy.[28,31] Whereas, for the Mo layer, the Cauchy's model provided the following fitting parameters: A = 4.55, B = -84.68, C = 53.85, D = 197253.35, E = -24.61 and F = 13.95.[31] More details about fitting procedure can be found elsewhere.[28,30] In brief, the measured ellipsometric spectra were fitted by minimizing the squared difference (χ^2) between the measured and calculated values of the ellipsometric parameters. Maximum number of iteration allowed was 100 and criterion for convergence used was $\delta\chi^2 = 0.000001$. In Fig. 5, the best fitted theoretical spectra are shown with the experimental spectra. The thicknesses of the three layers calculated from the fitting are also shown in the inset of Fig. 5. These values are in agreement with values calculated from the cross-sectional FESEM micrograph. Figure 6(a) shows the fractured cross-sectional FESEM micrograph of the HfO_x/Mo/HfO_2 coating deposited on Si substrate. The corresponding three-dimensional atomic force microscopy image is shown in Fig. 6 (b). The average root mean

square roughness of the HfO_x/Mo/HfO_2 coating deposited on Si substrate was approximately 2.0 nm.

The refractive indices and the extinction coefficients of the HfO_x, HfO_2 (layers 1 and 3) and Mo metal layer (layer 2) in the absorber coating are shown in Fig. 7, which are in good agreement with the values reported by other workers.[3,8] The *n* and *k* values of bottom HfO_x layer (layer 1; Fig. 7(a)) decreased monotonically with increasing wavelength. This shows that the bottom HfO_x layer exhibits an intermediate character, i.e., a transition between the dielectric and the metallic behavior. Whereas, the *n* value of the top HfO_2 layer (layer 3), shown in Fig. 7(b), was lower than that of the metallic Mo layer (Fig. 7(c)) and the bottom HfO_x layer (Fig. 7(a)). The *k* values for the top HfO_2 layer were almost zero (0.001-0.005) in the visible and near-IR regions, indicating its dielectric behavior. These data indicate that the top HfO_2 layer mainly acts as an antireflection coating. Fig. 7(c) shows the *n* and *k* values of Mo metal layer (layer 2). The *n* and *k* values of Mo metal layer increased with increasing wavelength, which confirms the metallic behavior of molybdenum.

In thin films, the absorption takes place mainly due to two mechanisms: i) interference induced absorption ii) intrinsic absorption. The interference induced absorption depends on the refractive index of the coating, whereas the intrinsic absorption depends on the extinction coefficient of the coating. In HfO_x/Mo/HfO_2 coating, the *n* and *k* values are high for the Mo metal layer and the absorption in the Mo metal layer is mainly due to a combination of interference effect and intrinsic absorption. Whereas, for the bottom HfO_x layer the *n* is high and the *k* is low in the wavelength range of 350-1200 nm. Therefore, for the bottom HfO_x layer the absorption depends mainly on interference mechanism than intrinsic absorption. These results

clearly showed that the interference induced absorption plays a major role in the absorption of the multilayer absorber coating.

From the k values, we calculated the absorption coefficients (β) for all the three layers, which are shown in Fig. 8. The β values were calculated from:

$$\beta = 4\pi k/\lambda. \quad (1)$$

For the top HfO_2 layer (Fig. 8(a)), the β values were low in the visible (e.g., 1.2×10^3 cm^{-1} at 400 nm) and near-IR regions (e.g., 1.0×10^2 cm^{-1} at 1200 nm) when compared to the bottom HfO_x layer (Fig. 8(b)). For the bottom HfO_x layer (Fig. 8(b)), the β values were high in the visible region (e.g., 6.4×10^4 cm^{-1} at 400 nm) and relatively low in the near-IR region (4.8×10^3 cm^{-1} at 1200 nm), indicating its high absorption in the visible region. Whereas, for the Mo layer, the β values were high in both visible (3.0×10^5 cm^{-1} at 400 nm) and near-IR regions (1.8×10^5 cm^{-1} at 1200 nm) when compared to the HfO_x and HfO_2 layers. These results indicate that the main contribution to absorption in the HfO_x/Mo/HfO_2 multilayer absorber coating is due to the semitransparent Mo metal layer and the bottom HfO_x layer.

F. Thermal stability in air

In order to study the thermal stability of the HfO_x/Mo/HfO_2 multilayer absorbers, the coatings were heat-treated in air at different temperatures for 2 h. The absorptance and the emittance values of the heat-treated HfO_x/Mo/HfO_2 multilayer absorber are listed in Table II. It is clear from the Table II that for HfO_x/Mo/HfO_2 coatings, the absorptance and the emittance values did not change significantly even after heat-treatment at 400°C for 2 h. At T_A = 425°C, the absorptance value decreased ($\Delta\alpha$ = -0.111) and the emittance value increased ($\Delta\varepsilon$ = +0.05) significantly. This is because at temperatures greater than 350°C, copper from the substrate starts diffusing into the coating and its subsequent oxide formation results in optical degradation

in the visible range and decrease of solar absorptance.[31] Therefore, the $HfO_x/Mo/HfO_2$ coating on Cu substrate is thermally stable in air up to 400°C with a solar selectivity of 0.893/0.07.

In order to avoid the diffusion of copper into the coating, approximately 40 nm thick Mo interlayer was deposited on copper substrate. The addition of Mo interlayer in the multilayer absorber coating has no significant effect in the absorptance and the emittance values. It has been reported that the molybdenum acts as a diffusion barrier for copper up to 600°C.[32] The absorptance and the emittance values of the heat-treated $Mo/HfO_x/Mo/HfO_2$ multilayer absorber are listed in Table III. It is clearly evident from the table that the Mo interlayer acts as a diffusion barrier for copper which resulted in increase in the thermal stability of the coating up to 500°C. At $T_A > 500$°C, the absorptance value decreased ($\Delta\alpha = -0.161$) and the emittance value increased drastically ($\Delta\varepsilon = +0.26$). This degradation was due to the oxidation of Mo present in the coating and also due to the formation of a new phase (i.e., $HfMo_2O_8$) which was formed by the reaction between MoO_3/MoO_2 and HfO_2.[33] This was confirmed using Raman spectroscopy and will be discussed later.

The $Mo/HfO_x/Mo/HfO_2$ multilayer absorber coating deposited on Cu substrates delaminated completely at temperatures greater than 525°C in air. Therefore, in order to test the structural stability of the multilayer absorber at higher temperatures, the coatings were deposited on SS substrates with Mo interlayer and were heat-treated in air for 2 h at different temperatures in the range of 400-525°C. The absorptance and the emittance values of the heat-treated coatings are shown in Table IV. At $T_A = 525$°C, the absorptance value decreased drastically ($\Delta\alpha = -0.142$) and the emittance value decreased slightly ($\Delta\varepsilon = -0.03$). The coatings deposited on SS substrates were also degraded completely at 525°C, the reason for which has been explained earlier.

The changes in the chemical composition of $Mo/HfO_x/Mo/HfO_2$ coating at higher operating temperatures were studied using micro-Raman spectroscopy. The composite Raman spectra of the as-deposited and multilayer absorbers deposited on Cu substrates heat-treated up to 525°C are shown in Fig. 9. The shape of Raman spectra did not change significantly even after heating the sample up to a temperature of 400ºC, indicating the stable composition/microstructure of the multilayer coatings. At T_A= 500 ºC, six new bands centered at 193, 260, 322, 442, 536 and 728 cm^{-1} were observed (see inset in Fig. 9). The bands centered at 260 and 322 cm^{-1} correspond to A_g symmetry and band centered at 536 cm^{-1} corresponds to B_g symmetry of *m*-HfO_2.[23] Whereas, bands centered at 442 and 728 cm^{-1} is attributed to vibrations of *m*-MoO_2.[34] The oxidation of Mo at 500ºC resulted in slight decrease in the solar absorptance ($\Delta\alpha$ = -0.038, see Table III). At T_A= 525ºC, two new bands centered at 87 and 878 cm^{-1} were observed, which are attributed to the formation of $HfMo_2O_8$ due to the reaction between HfO_2 and MoO_2/MoO_3.[33] The compound $HfMo_2O_8$ can form very easily from the above reaction as the standard Gibb's free energies of formation of $HfMo_2O_8$ from HfO_2+MoO_3 and HfO_2+MoO_2 are reported to be -1837.89 and -1877.30 kJ/mol, respectively.[35,36] The formation of this new phase resulted in degradation of the multilayer absorber coating. At T_A= 525ºC, the absorptance decreased (($\Delta\alpha$ = -0.161) and the emittance increased drastically ($\Delta\varepsilon$ = +0.26, see Table III).

The Raman spectra of as-deposited $Mo/HfO_x/Mo/HfO_2$ multilayer absorbers deposited on SS substrates and coatings heat-treated up to 525°C in air are shown in Fig. 10. The spectrum of as-deposited coating (Fig. 10 (a)) shows four broad bands centered at 95, 152, 284 and 563 cm^{-1} correspond to A_g symmetry of *m*-HfO_2. The deconvoluted Raman spectrum of as-deposited coating is shown in the inset. At T_A = 500°C (Fig. 10(b)), bands centered at 452, 719 and 819 cm^{-1} were observed which originate due to vibrations of *m*-MoO_2 and *m*-MoO_3.[34,37] Whereas,

the bands centered at 139, 179, 242 and 631 cm^{-1} correspond to B_g symmetry of HfO_2. At T_A = 525°C (Fig. 10 (c)), three characteristic Raman peaks of molybdenum oxide were observed. These Raman bands are assigned to the terminal oxygen (Mo=O) stretching mode at 992 cm^{-1}, the triply connected bridge-oxygen (Mo_3-O) stretching mode at 661 cm^{-1}, and the doubly connected bridge-oxygen (Mo_2-O) stretching mode at 815 cm^{-1}.[37] For a comparison, the Raman spectrum of MoO_3 (heat-treated Mo in air at 500°C for 2 h) is shown in the inset. The formation of $HfMo_2O_8$ is clearly evident from the peaks centered at 770 and 942 cm^{-1}.

These results indicated that the fine Mo crystallites in the $Mo/HfO_x/Mo/HfO_2$ coating oxidized in air at 500ºC and the Mo metal content, responsible for the intrinsic optical absorption, decreases, resulting in a decrease in the solar absorptance. In addition, at $T_A \geq 500$ °C the formation of a new phase due to the reaction of MoO_3/MoO_2 with HfO_2, i.e., $HfMo_2O_8$ (as evident from the Raman data) resulted in a decrease in the absorptance.[33] It is believed that the formation of $HfMo_2O_8$ leads to crack formation, delamination, and subsequent oxidation of the coating because of the large difference in the thermal expansion coefficients of $HfMo_2O_8$ (-4.0×10^{-6}/°C), HfO_2 (3.8×10^{-6}/°C) and Cu substrate (16.5×10^{-6}/°C).[31,33]

G. Thermal stability in vacuum

In addition to the oxide formation, heating of the multilayer absorber in air also leads to phase transformation. Both the phase transformation and the presence of oxides affect the nature of the Raman spectra. In order to study whether the coatings were stable at higher annealing temperatures, they were heated under high vacuum (5.0×10^{-4} Pa) for 2 h at different temperatures. The absorptance and the emittance values of the $Mo/HfO_x/Mo/HfO_2$ coatings deposited on Cu and SS substrates after heat-treatment are listed in Table V and VI, respectively. For coatings deposited on Cu substrates, even after heat-treatment up to 800ºC, there was no

measurable change in the emittance but a slight decrease ($\Delta\alpha$ = -0.024) in the absorptance was observed as a result of vacuum annealing. Whereas, for coatings deposited on SS substrates, the absorptance decreased ($\Delta\alpha$ = -0.033, at T_A = 800 ºC) and no significant change in the emittance ($\Delta\varepsilon$ = +0.01) was observed. Fig. 11 shows the deconvoluted Raman spectra of as-deposited and vacuum annealed Mo/HfO_x/Mo/HfO_2 coatings deposited on Cu substrates. It is quite clear from the spectra that annealing of the Mo/HfO_x/Mo/HfO_2 coatings in vacuum up to 800 ºC did not change the nature of the Raman spectra. These results are in agreement with the absorptance and emittance data.

IV. Conclusions

The HfO_x/Mo/HfO_2 multilayer absorber coatings deposited on Cu substrates exhibited high solar absorptance (α = 0.905-0.923) and low thermal emittance (ε = 0.07-0.09). The XRD data indicated the presence of *m*- and *t*-HfO_2 in the HfO_x/Mo/HfO_2 multilayer absorber coating. The optical constants of HfO_x, Mo and HfO_2 layers measured from the ellipsometric data clearly showed that the Mo and the HfO_x layers are the main absorber layers and the top HfO_2 layer acts as an antireflection coating. The HfO_x/Mo/HfO_2 coatings deposited on Cu substrates were thermally stable up to 400°C for 2 h in air. Above 400°C, the absorptance value decreased drastically due to diffusion of Cu from the substrate and its subsequent oxide formation. Whereas, Mo/HfO_x/Mo/HfO_2 multilayer absorber coatings on Cu substrates were stable up to 500°C in air (2 h) with a solar selectivity of 0.872/0.09. This result clearly showed that the Mo (40 nm) layer acts as a diffusion barrier for Cu. The Mo/HfO_x/Mo/HfO_2 coatings deposited on SS substrates were also stable up to 500°C with a solar selectivity of 0.874/0.15. The oxidation of the Mo at 500°C and the formation of MoO_3/MoO_2 and $HfMo_2O_8$ phases at 525°C resulted in degradation of the multilayer absorber coatings. The micro-Raman spectroscopy data confirmed

the formation of MoO_2/MoO_3 and $HfMo_2O_8$ at temperatures ≥ 500°C for coatings deposited on both Cu and SS substrates. Vacuum annealing studies of $Mo/HfO_x/Mo/HfO_2$ coatings showed marginal changes in the absorptance and emittance values up to 800°C. The compositional stability of the coatings in air (up to 500°C) and vacuum (up to 800°C) was confirmed using Raman spectroscopy.

Acknowledgements

The authors thank the Director, NAL (CSIR) for giving permission to publish these results. Financial support from Ministry of New and Renewable Energy, New Delhi is acknowledged.

TABLE I: Optical parameters of HfO_2 and HfO_x layers extracted using spectroscopic ellipsometry by employing Adachi model.

Fitting Parameters	HfO_2	HfO_x
$\varepsilon(\infty)$	0.69	1.28
E_0	5.82 eV	3.90 eV
Γ_0	0.068 eV	1.61 eV
A_0	101.05 $eV^{1.5}$	63.47 $eV^{1.5}$
A_{0x}	0.0073 eV	0.0073 eV
G_0	0.064 eV	0.064 eV

Table II. Effect of 2 h annealing (in air) on the absorptance and emittance values of $HfO_x/Mo/HfO_2$ coatings deposited on copper substrates.

Annealing Temperature (ºC)	α			∈		
	As-deposited	Annealed	Δα	As-deposited	Annealed	Δ∈
400	0.917	0.893	-0.024	0.07	0.07	0.00
425	0.913	0.802	-0.111	0.07	0.12	+0.05
500	0.916	0.611	-0.305	0.06	0.28	+0.22

Table III. Effect of 2 h annealing (in air) on the absorptance and emittance values of $Mo/HfO_2/Mo/HfO_2$ coatings deposited on copper substrates.

Annealing Temperature (ºC)	α			∈		
	As-deposited	Annealed	Δα	As-deposited	Annealed	Δ∈
200	0.918	0.917	-0.001	0.08	0.08	0.00
300	0.922	0.914	-0.008	0.09	0.10	+0.01
400	0.922	0.898	-0.024	0.07	0.08	+0.01
500	0.910	0.872	-0.038	0.09	0.09	0.00
525	0.922	0.761	-0.161	0.09	0.35	+0.26

Table IV. Effect of 2 h annealing (in air) on the absorptance and emittance values of $Mo/HfO_2/Mo/HfO_2$ coatings deposited on SS substrates.

Annealing Temperature (ºC)	α			∈		
	As-deposited	Annealed	Δα	As-deposited	Annealed	Δ∈
400	0.908	0.904	-0.004	0.17	0.17	0.00
500	0.902	0.874	-0.028	0.17	0.15	-0.02
525	0.914	0.772	-0.142	0.17	0.14	-0.03

Table V. Effect of 2 h annealing (in vacuum) on the absorptance and emittance values of $Mo/HfO_2/Mo/HfO_2$ coatings deposited on copper substrates.

Annealing Temperature (ºC)	α			∈		
	As-deposited	Annealed	Δα	As-deposited	Annealed	Δ∈
500	0.923	0.923	0.000	0.09	0.08	-0.01
600	0.919	0.919	0.000	0.08	0.08	0.00
700	0.919	0.899	-0.020	0.08	0.07	-0.01
800	0.917	0.893	-0.024	0.08	0.08	0.00

Table VI. Effect of 2 h annealing (in vacuum) on the absorptance and emittance values of $Mo/HfO_2/Mo/HfO_2$ coatings deposited on SS substrates.

Annealing Temperature (ºC)	α			∈		
	As-deposited	Annealed	Δα	As-deposited	Annealed	Δ∈
600	0.917	0.894	-0.023	0.17	0.12	-0.05
700	0.911	0.890	-0.021	0.16	0.13	-0.03
800	0.912	0.879	-0.033	0.16	0.17	+0.01

Figure Captions

FIG. 1. Schematic diagram of the $HfO_x/Mo/HfO_2$ multilayer absorber coating deposited on copper substrate.

FIG. 2. XRD patterns of (a) single layer HfO_2 coating deposited on Si substrate at an O_2 flow rate of 8 sccm (b) a typical $HfO_x/Mo/HfO_2$ multilayer absorber coating deposited on Si substrate.

FIG. 3. Raman spectra of: (a) single layer HfO_2 coating deposited on Si substrate at an oxygen flow rate of 8 sccm and (b) $HfO_x/Mo/HfO_2$ multilayer absorber coating deposited on Cu substrate. The inset shows the deconvoluted Raman spectrum of $HfO_x/Mo/HfO_2$ multilayer absorber coating.

FIG. 4. Core level XPS spectra of: (a) Hf 4*f*, (b) Hf 4*d* and (c) O 1*s* for the as-deposited HfO_x coating deposited at an O_2 flow rate of 6 sccm (layer 1). Also shown is the core level XPS spectra of: (d) Hf 4*f*, (e) Hf 4*d* and (f) O 1*s* for the HfO_2 coating deposited at an O_2 flow rate of 8 sccm (layer 3).

FIG. 5. Variations of experimentally determined ψ and Δ values with wavelength along with best-fit theoretical curves for the optimized $HfO_x/Mo/HfO_2$ coating deposited on Cu substrate. The dotted lines represent theoretical fits to the experimental data.

FIG. 6. (a) FESEM cross-sectional micrograph of $HfO_x/Mo/HfO_2$ coating deposited on Si substrate and (b) three-dimensional AFM image of $HfO_x/Mo/HfO_2$ coating deposited on Si substrate.

FIG. 7. Variations of experimentally determined *n* and *k* values for (a) HfO_x (layer 1), (b) HfO_2 (layer 3) and (c) Mo (layer 2).

FIG. 8. Variations of absorption coefficients for (a) HfO_2 layer, (b) HfO_x layer and (c) Mo layer.

FIG. 9. Composite Raman spectra of as-deposited Mo/HfO_x/Mo/HfO_2 coating on Cu substrate and coatings heat-treated up to 525°C for 2 h in air. Also shown in the inset is the deconvoluted Raman spectrum of coating heat-treated at 500°C.

FIG. 10. Composite Raman spectra of as-deposited Mo/HfO_x/Mo/HfO_2 coating on SS substrate and coatings heat-treated up to 525°C for 2 h in air. Also shown in the insets are the deconvoluted Raman spectrum of as-deposited coating and Raman spectrum of MoO_3.

FIG. 11. Deconvoluted Raman spectra of: (a) as-deposited Mo/HfO_x/Mo/HfO_2 coating on Cu substrate and coatings vacuum annealed at (b) 600°C, (c) 700°C and (d) 800°C for 2 h.

References

[1]*Solar Energy Conversion: Solid State Physics Aspects: Topics in Applied Physics*, edited by B.O. Seraphin (Springer, Berlin, 1979) Vol. 31.

[2]M. Ritala, M. Leskela, L. Niinisto, T. Prohaska, G. Friedbacher and M. Grasserbauer, Thin Solid Films **250**, 72 (1994).

[3]M. F. Al-Kuhaili, Opt. Mater. **27**, 383 (2004).

[4]M. Lesser, Opt. Eng. **26**, 911 (1987).

[5]M. Fadel, O. A. Azim, O. A. Omer, and R. R. Basily, Appl. Phys. A: Mater. Sci. Process. **66**, 335 (1998).

[6]M. Zukic, D. G. Torr, J. F. Spann, M. R. Torr, Applied Optics **29**, 4284 (1990).

[7]S. M. Edlou, A. Smajkiewicz, G. A. Al-Jumaily, Applied Optics **32**, 5601 (1993).

[8]J. M. Khoshman, M. E. Kordesch, Surf. Coat. Technol. **201**, 3530 (2006).

[9]J-W. Park, D-K. Lee, D. Lim, H. Lee and S-H. Choi, J. Appl. Phys. **104**, 033521 (2008).

[10]M. T. Luque, E. S. Andres, A. d. Prado, I. Martil, M. L. Lucia and G. G. Diaz, J. Appl. Phys. **102**, 044106 (2007).

[11]V. Pervak, F. Krausz and A. Apolonski, Thin Solid Films **515**, 7984 (2007).

[12]S. V. Ushakov, A. Navrotsky, Y. Yang, S. Stemmer, K. Kukli, M. Ritala, M. A. Leskela, P. Fejes, A. Demkov, C. Wang, B.-Y. Nguyen, D. Triyoso and P. Tobin, Phys. Stat. Sol. (B) **241**, 2268 (2004).

[13]Q. Fang, J.-Y. Zhang, Z. Wang, M. Modreanu, B. J. O'Sullivan, P. K. Hurley, T. L. Leedham, D. Hywel, M. A. Audier, C. Jimenez, J.-P. Senateur and I. W. Boyd, Thin Solid Films **453-454,** 203 (2004).

[14]H.C. Barshilia and K.S. Rajam, Surf. Coat. Technol. **201**, 329 (2006).

[15]H.C. Barshilia and K.S. Rajam, J. Mater. Res. **19**, 3196 (2004).

[16]O.S. Heavens, *Optical Properties of Thin Solid Films* (Dover, New York, 1965).

[17]E.E. Chain, G. E. Carver and B.O. Seraphin, Thin Solid Films **72,** 59 (1980).

[18]X. Luo, A.A. Demkov, D. Triyoso, P. Fejes, R. Gregory and S. Zollner, Phys. Rev. B **78,** 245314 (2008) .

[19]Joint Committee on Powder Diffraction Standards, File No. 06-0318.

[20]Joint Committee on Powder Diffraction Standards, File No. 08-0342.

[21]X. Zhao and D. Vanderbilt, Phys. Rev. B, 65, 233106 (2002).

[22]H. Fujimori, M. Yashima, M. Kakihana and M. Yoshimura, J. Am. Ceram. Soc. **84,** 663 (2001).

[23]E. Anastassakis, B. Papanicolaou and I. M. Asher, J. Phys. Chem. Solids **36**, 667 (1975).

[24]G. He, M. Liu, L. Q. Zhu, M. Chang, Q. Fang and L. D. Zhang, Surf. Sci. **576**, 67 (2005).

[25]S. Q. Wang, J. W. Mayer, J. Appl. Phys. **64,** 4711 (1988).

[26]S. Ninomiya and S. Adachi, J. Appl. Phys. **78**, 1183 (1995).

[27]S. Adachi, H. Mori, and S. Ozaki, Phys. Rev. B **66**, 153201 (2002).

[28]D. Bhattacharyya and A. Biswas, J. Appl. Phys. **97,** 053501 (2005).

[29]N.K. Sahoo, S. Thakur, M. Senthilkumar, D. Bhattacharyya, N.C. Das, Thin Solid Films **440**, 155 (2003).

[30]A. Biswas, D. Bhattacharyya, H.C. Barshilia, N. Selvakumar and K.S. Rajam, Appl. Surf. Sci. **254,** 1694 (2008).

[31]H. C. Barshilia, N. Selvakumar, K. S. Rajam and A. Biswas, J. Appl. Phys. **103,** 023507 (2008).

[32]Y. He and J. Y. Feng, J. Cryst. Growth **263,** 203 (2004).

[33]C. A. Kennedy, M. A. White, A. P. Wilkinson and T. Varga, Phys. Rev. B. 75, 224302 (2007).

[34]R. Prakash, D. M. Phase, R. J. Choudhary and R. Kumar, J. Appl. Phys. **103,** 043712 (2008).

[35]Z. Singh, S. Dash, R. Prasad and V. Venugopal, J. Alloys Compd. **244,** 85 (1996).

[36]M. S. Samant, S. R. Bharadwaj, A. S. Kerkar and S. R. Dharwadkar, J. Nucl. Mater. 207, 98 (1993).

[37]K. Ajito, L. A. Nagahara, D. A. Tryk, K. Hashimoto and A. Fujishima, J. Phys. Chem. **99**, 16383 (1995).

Fig. 1

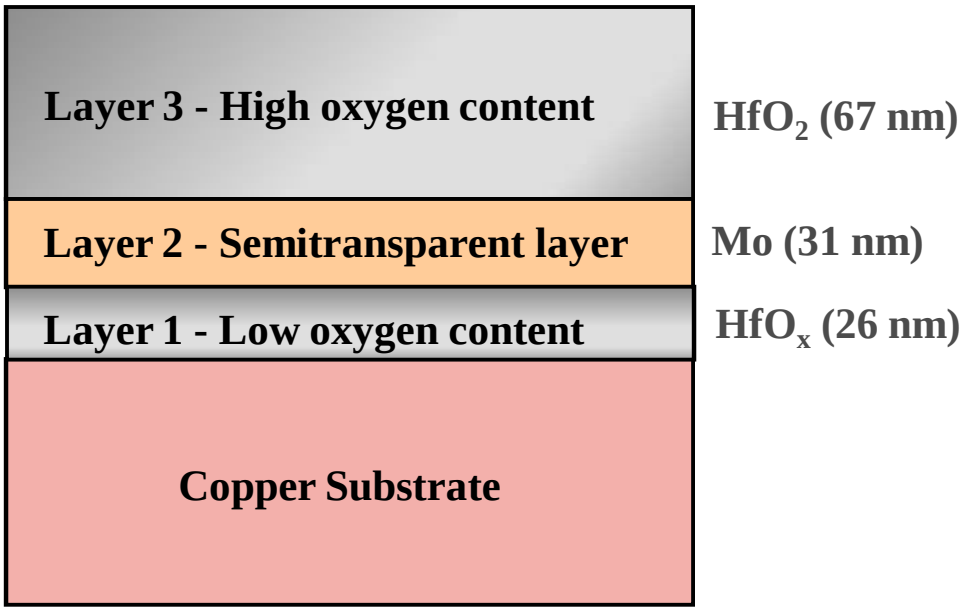
Layer 3 - High oxygen content
HfO2 (67 nm)
Layer 2 - Semitransparent layer
Mo (31 nm)
Layer 1 - Low oxygen content
HfOx (26 nm)
Copper Substrate

Fig. 2.

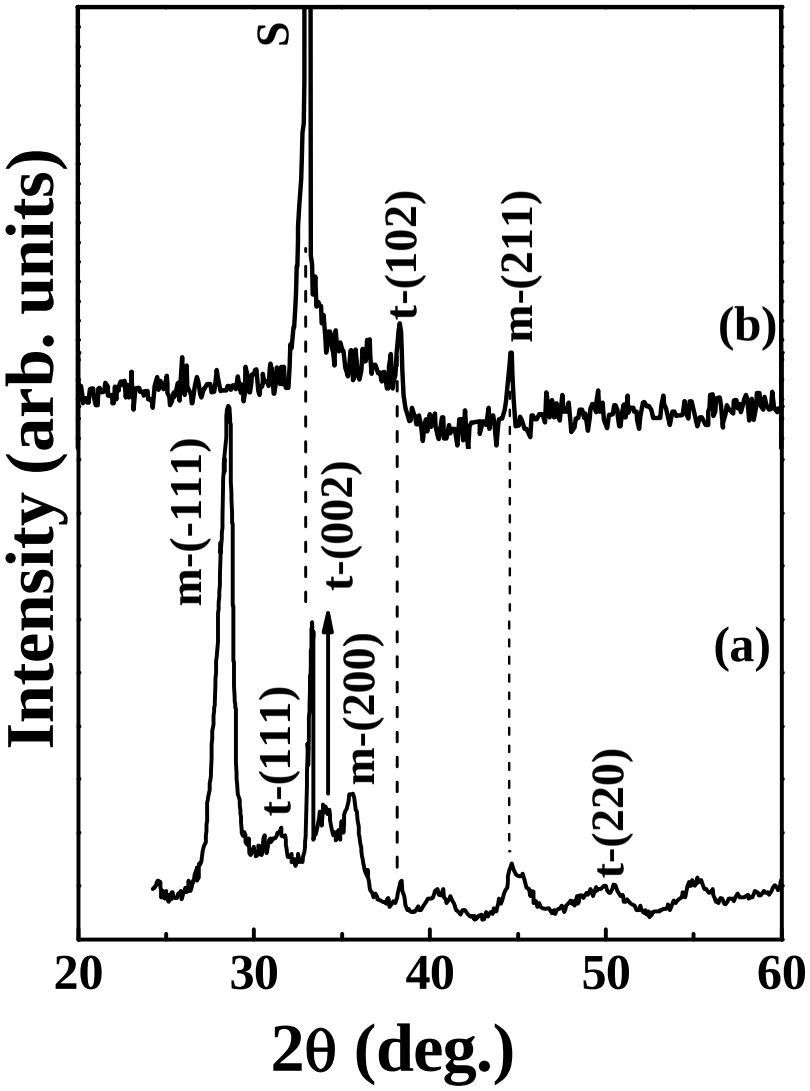
Intensity (arb. units)
2θ (deg.)
20
30
40
50
60
S
t-(102)
m-(211)
(b)
m-(-111)
t-(002)
t-(111)
m-(200)
t-(220)
(a)

Fig. 3.

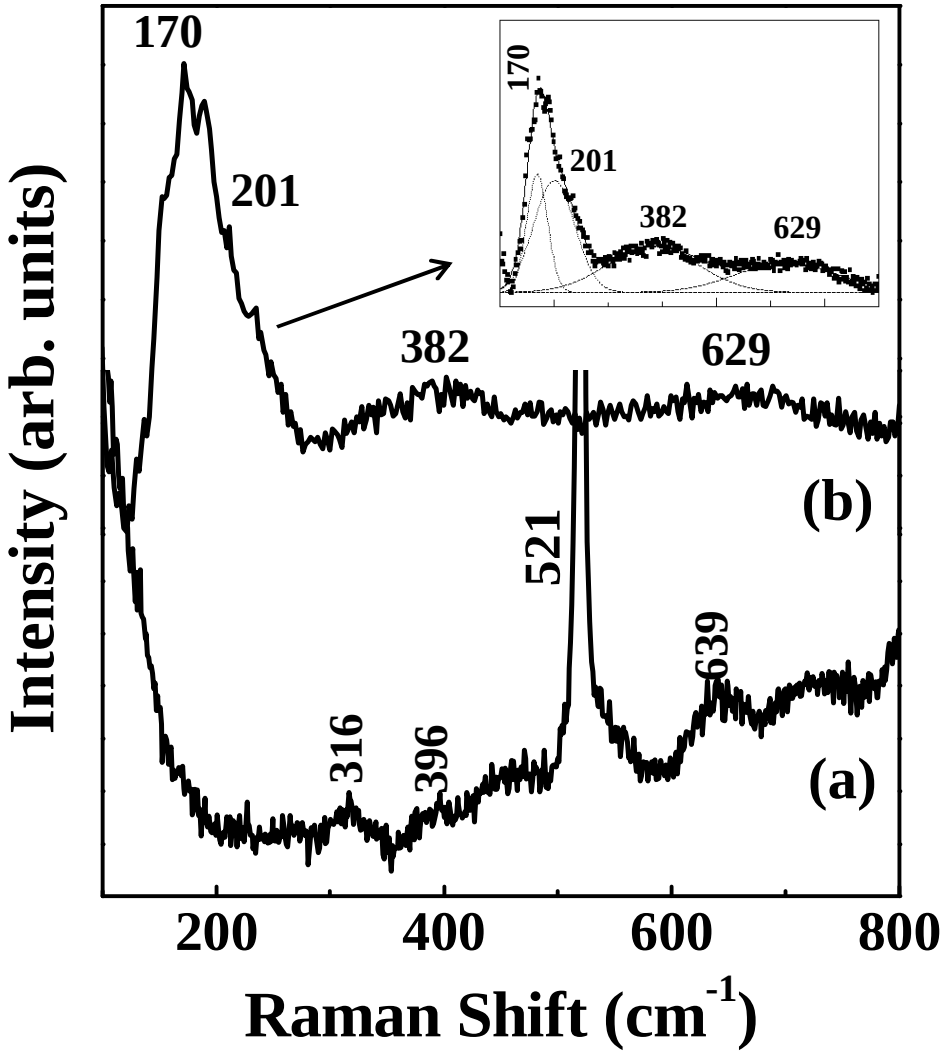
170
201
382
629
521
639
316
396
(b)
(a)
Intensity (arb. units)
200
400
600
800
Raman Shift (cm-1)

Fig. 4

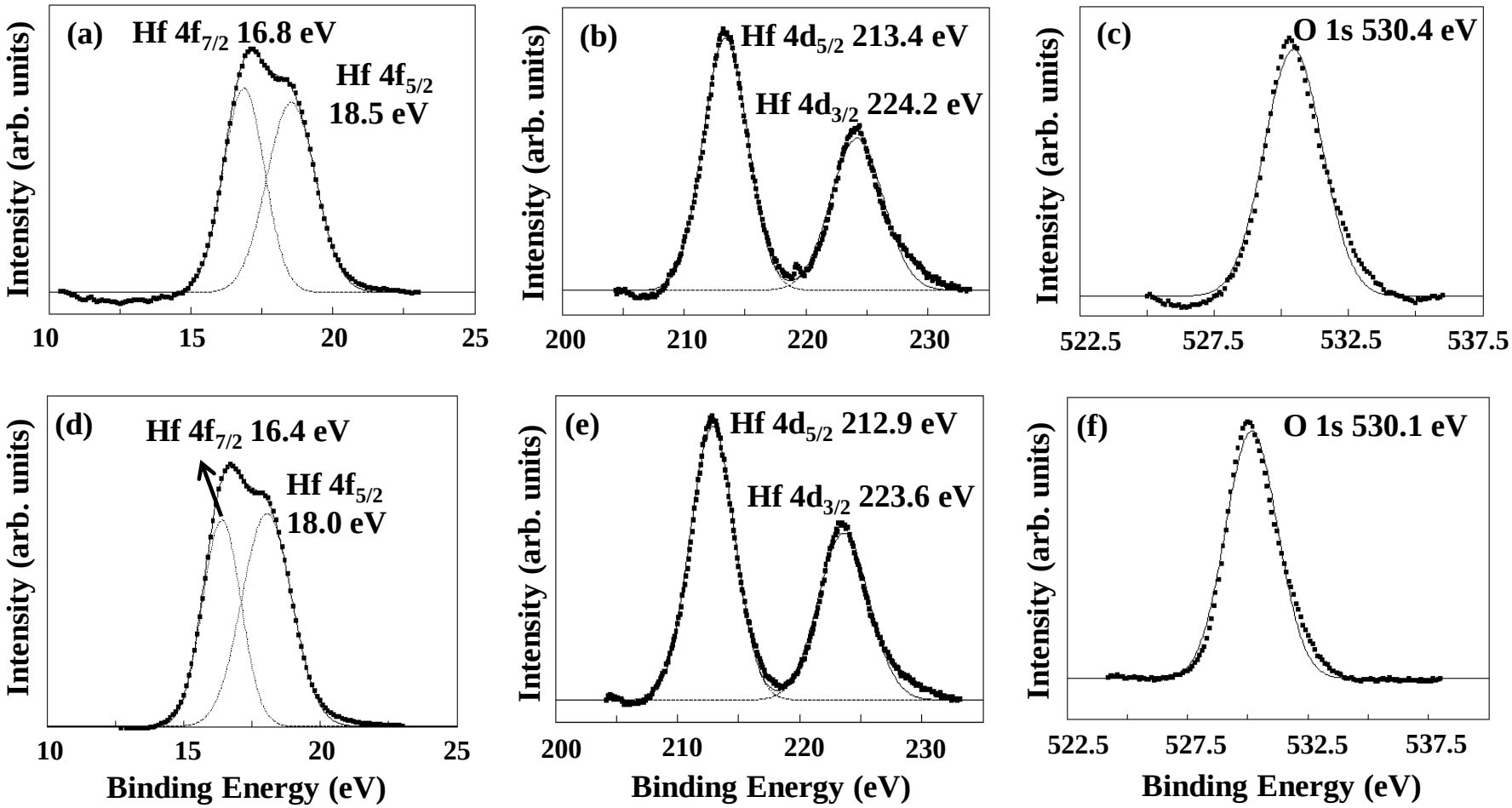
(a) Hf 4f7/2 16.8 eV
Hf 4f5/2
18.5 eV
(b) Hf 4d5/2 213.4 eV
Hf 4d3/2 224.2 eV
(c) O 1s 530.4 eV
(d) Hf 4f7/2 16.4 eV
Hf 4f5/2
18.0 eV
(e) Hf 4d5/2 212.9 eV
Hf 4d3/2 223.6 eV
(f) O 1s 530.1 eV
Intensity (arb. units)
Binding Energy (eV)
10
15
20
25
200
210
220
230
522.5
527.5
532.5
537.5

Fig. 5

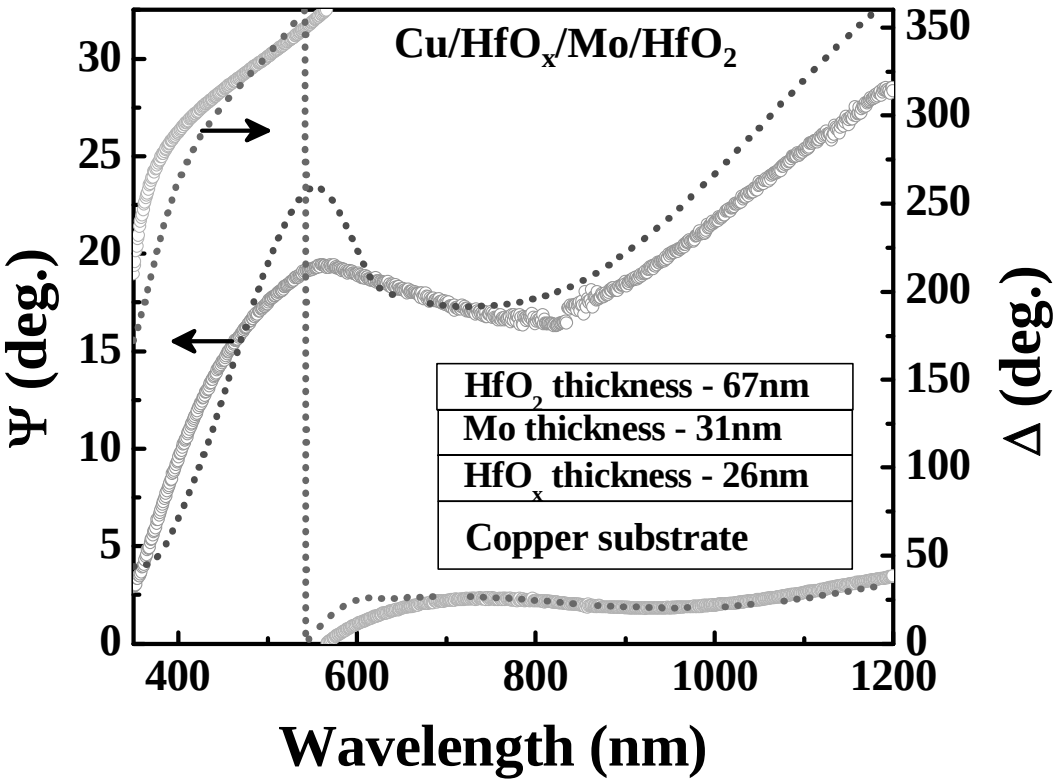
Cu/HfO$_x$/Mo/HfO$_2$
HfO$_2$ thickness - 67nm
Mo thickness - 31nm
HfO$_x$ thickness - 26nm
Copper substrate
Ψ (deg.)
Δ (deg.)
Wavelength (nm)
0
5
10
15
20
25
30
0
50
100
150
200
250
300
350
400
600
800
1000
1200

Fig. 6

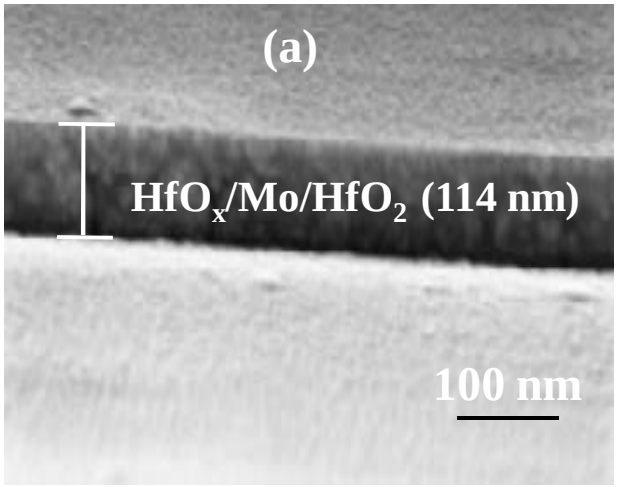
(a)
HfO_x/Mo/HfO_2 (114 nm)
100 nm

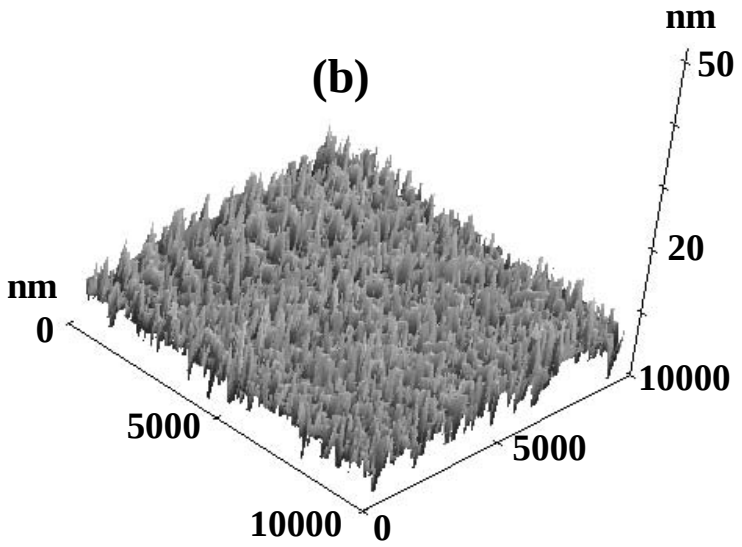
(b)
nm
50
20
10000
5000
0
nm
0
5000
10000
5000
0

Fig. 7

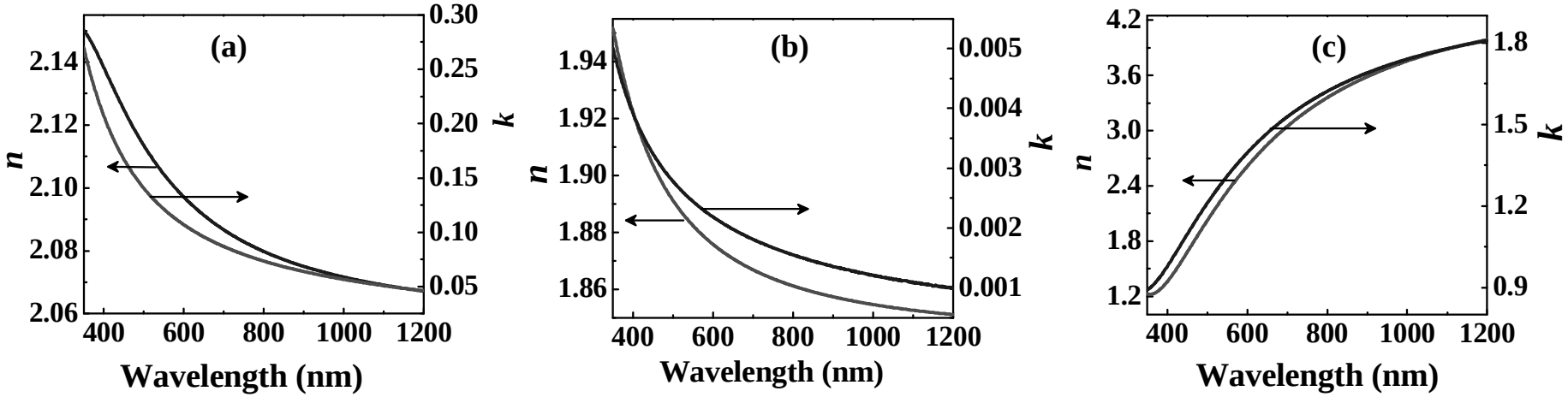
(a)
n
k
2.14
2.12
2.10
2.08
2.06
0.30
0.25
0.20
0.15
0.10
0.05
400
600
800
1000
1200
Wavelength (nm)
(b)
n
k
1.94
1.92
1.90
1.88
1.86
0.005
0.004
0.003
0.002
0.001
400
600
800
1000
1200
Wavelength (nm)
(c)
n
k
4.2
3.6
3.0
2.4
1.8
1.2
1.8
1.5
1.2
0.9
400
600
800
1000
1200
Wavelength (nm)

Fig. 8

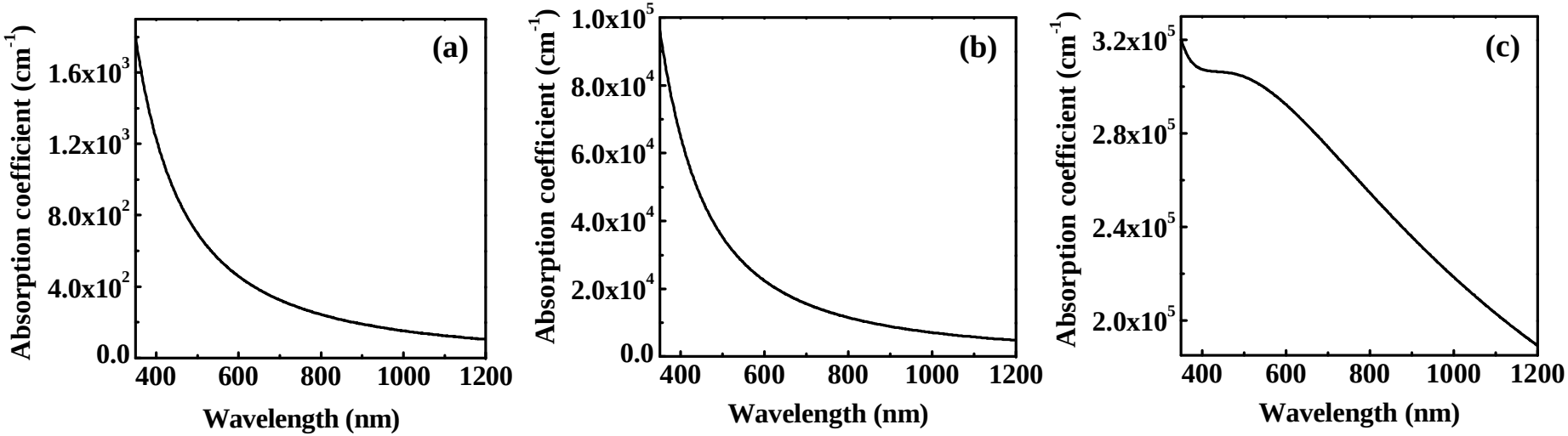
(a)
Absorption coefficient (cm-1)
1.6x10^3
1.2x10^3
8.0x10^2
4.0x10^2
0.0
400
600
800
1000
1200
Wavelength (nm)
(b)
Absorption coefficient (cm-1)
1.0x10^5
8.0x10^4
6.0x10^4
4.0x10^4
2.0x10^4
0.0
400
600
800
1000
1200
Wavelength (nm)
(c)
Absorption coefficient (cm-1)
3.2x10^5
2.8x10^5
2.4x10^5
2.0x10^5
400
600
800
1000
1200
Wavelength (nm)

Fig. 9

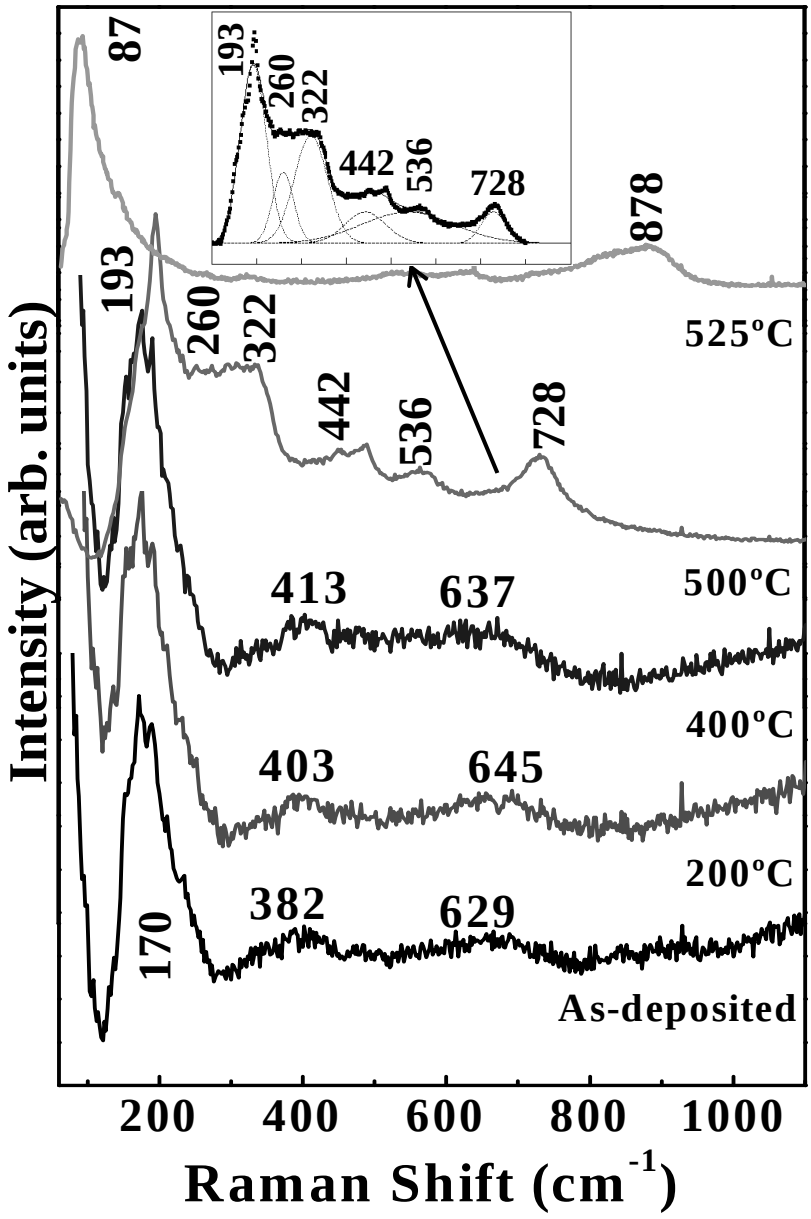
Intensity (arb. units)
Raman Shift (cm-1)
200
400
600
800
1000
87
193
260
322
442
536
728
878
525ºC
500ºC
413
637
400ºC
403
645
200ºC
382
629
170
As-deposited

Fig. 10

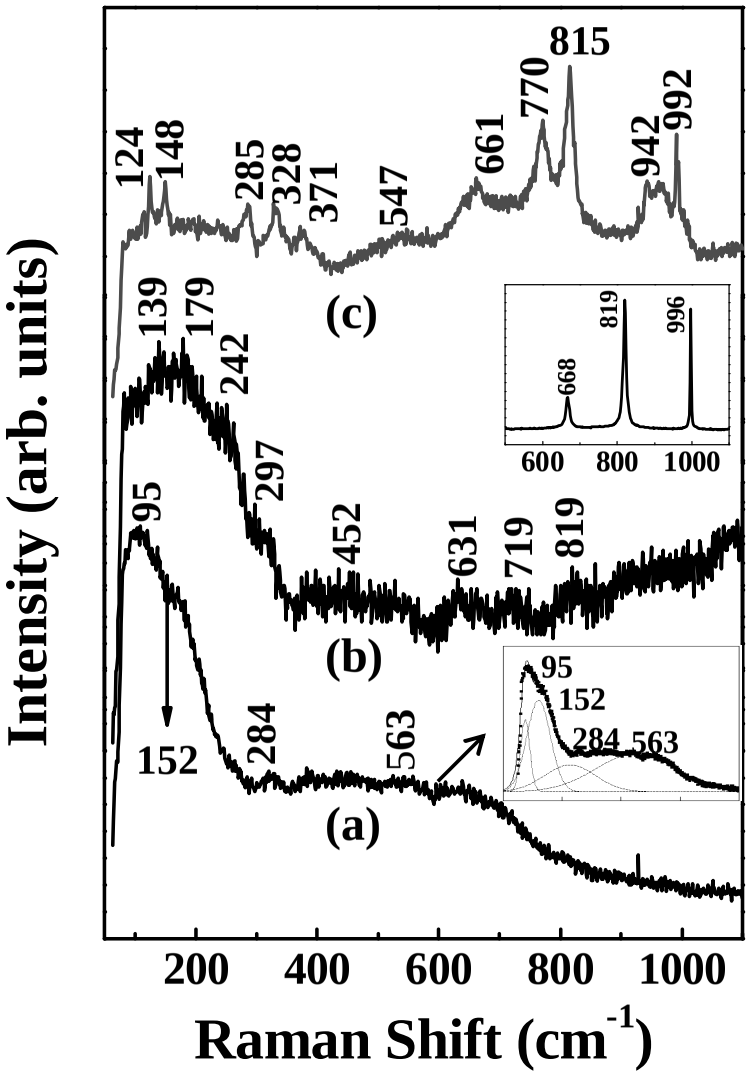
Intensity (arb. units)
Raman Shift (cm-1)
200
400
600
800
1000
124
148
285
328
371
547
661
770
815
942
992
(c)
139
179
242
297
452
631
719
819
(b)
95
152
284
563
(a)
668
819
996
600
800
1000
95
152
284
563

Fig. 11

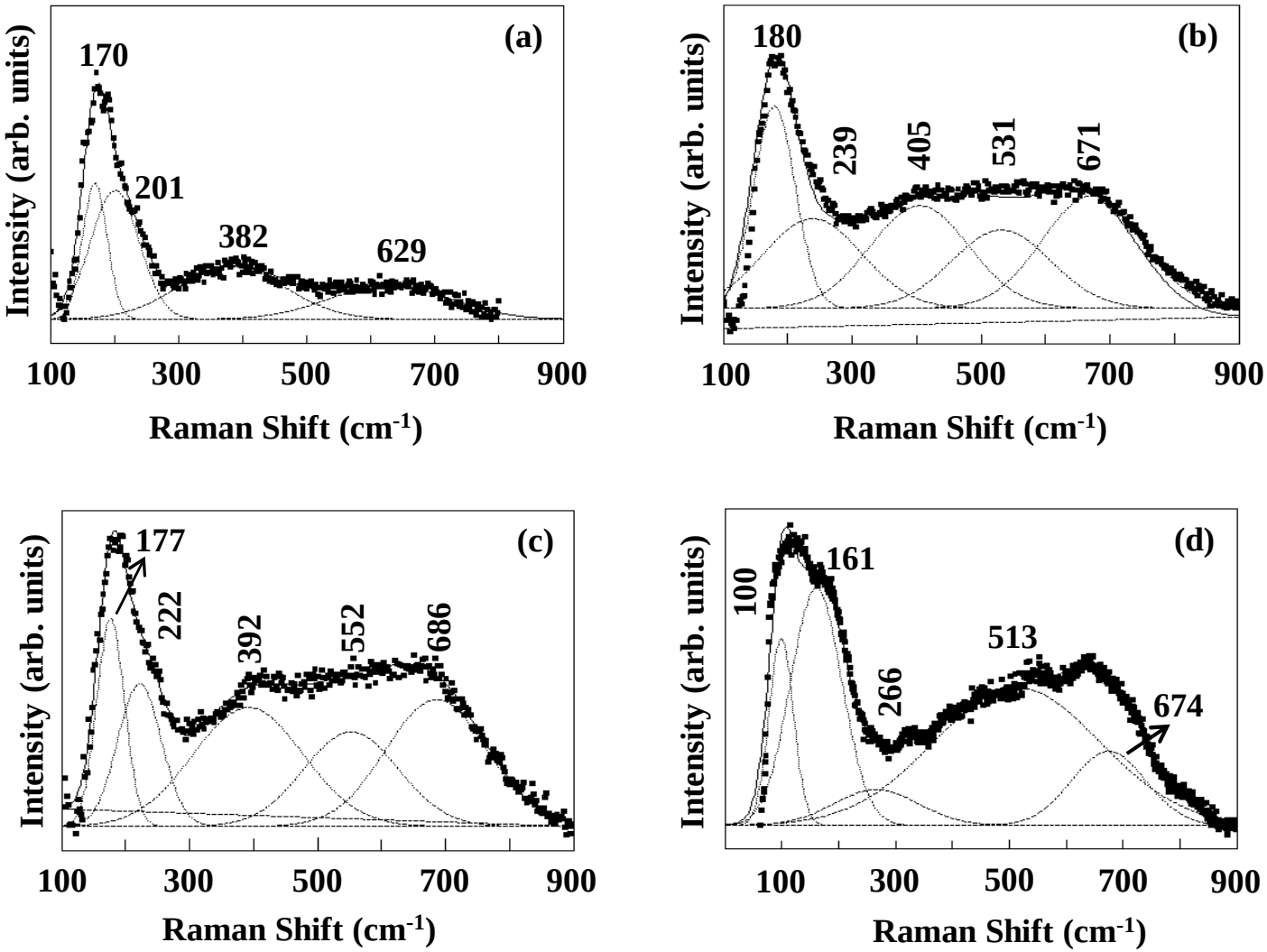
(a)
170
201
382
629
Intensity (arb. units)
100
300
500
700
900
Raman Shift (cm-1)
(b)
180
239
405
531
671
Intensity (arb. units)
100
300
500
700
900
Raman Shift (cm-1)
(c)
177
222
392
552
686
Intensity (arb. units)
100
300
500
700
900
Raman Shift (cm-1)
(d)
100
161
266
513
674
Intensity (arb. units)
100
300
500
700
900
Raman Shift (cm-1)